Long-Range Electron Transfer through Ultrathin Polyelectrolyte Complex Films: a Hopping Model

Samir Abou Shaheen, Rachel L. Abbett, Khalil Akkaoui, and Joseph B. Schlenoff*

Department of Chemistry and Biochemistry

The Florida State University

Tallahassee, FL 32308 USA

E-mail: schlen@chem.fsu.edu

Accepted version Phys Chem C 2021

Abstract

Pinhole-free ultrathin films of polyelectrolyte complex assembled using layer-by-layer deposition were used to evaluate electron transfer from a redox species in solution to an electrode over the distance range 1 to 9 nm. Over this thickness, the polyelectrolytes employed wet the surface and the polymer molecules flatten to less than their equilibrium size in 3-dimensions. A decay constant β for current as a function of distance of about 0.3 nm⁻¹ placed this system in the regime expected for multistep hopping versus a one-step tunneling event. Discreet hopping sites within the films were identified as ferrocyanide ions with an equilibrium concentration of 0.032 M and an average separation of 3.7 nm. The Butler-Volmer (BV) expression for electron transfer as a function of overpotential was modified by distributing the applied voltage evenly amongst the hopping sites. This modified BV expression fit both the distance dependence and the applied potential dependence well, wherein the only freely adjustable parameter was the electron transfer coefficient. The finding that β is simply the inverse of the hopping range is consistent with previous conclusions that electrons within conjugated molecule sites are delocalized, or, for non-conjugated systems, spread over more than one repeat unit by lattice distortions.

Introduction

As features in electronic circuits, especially those based on molecules, shrink to less than 10 nm, the transport of electrons through nominally insulating materials has become of prime interest. Experimentally, the distance dependence of electron transport has been probed in 2D structures using an insulating film, commonly a self-assembled monolayer, on a metal surface and either a redox species attached or in solution, 1, 2, 3, 4, 5, 6 or another metal contact to complete the circuit. 7, 8, 9, 10 In 1-dimension, molecular spacers separate donor and acceptor molecules or nanoscale electrodes. 11, 12, 13, 14, 15, 16, 17, 18 The transport of electrons through nonconductors is historically broken down into coherent tunneling over "short" range (less than about 4 nm) and incoherent hopping over longer ranges. The primary feature used to distinguish between the two is the distance dependence of the electron transfer rate, k, which exhibits an exponential falloff with distance d, characterized by decay length β , $k = k_0 e^{-\beta d}$ for tunneling and a more linear inverse dependence on distance for hopping. Well-packed chains of saturated hydrocarbon yield β values of around 10 nm-1, whereas conjugated molecular "wires" have a much broader range of β between 0.1 and 4 nm-1. 12, 13 Long range electron transport through DNA is believed to be facilitated by stacking of base pairs. 3

Probing electron transport in the 1-100 nm range requires high-quality (pinhole free) conformal, rugged, insulating films of uniform thickness. Methods to produce pinhole-free films in the 1-10 nm thickness range include the use of self-assembled monolayers, ^{20, 21} vacuum evaporation, ²² chemical vapor deposition, ²³ and electrochemical polymerization. ^{24, 25} Polyelectrolyte multilayers, PEMUs, are conformal ultrathin films made *via* an iterative deposition of polycations and polyanions on substrates using the layer-by-layer (LBL) technique. ²⁶ The spontaneous complexation of oppositely charged polymers is entropically driven by the release of their counterions. ²⁷ LBL assembly provides an efficient way to obtain films that are useful for their tunable functionality and accurate thickness control with nm resolution.

Tunneling transport over short ranges has been extensively analyzed using well-packed self-assembled monolayers or molecular spacers. In almost all cases, electron transfer follows the expected $\exp(-\beta d)$ distance dependence. Transport over longer range has produced a more diverse set of results and analyses. The weaker distance dependence is usually analyzed in terms of a hopping model, where electrons are transferred with the aid of intermediate sites, which may be delocalized. However, mechanistic aspects for long-range electron transfer are still widely discussed.^{8, 28, 29, 30} In the present work, a PEMU system has been employed to produce exceptionally thin films to study electron transfer over the 1 - 9 nm range using the reversible redox species ferrocyanide. Modifications of classical Butler-Volmer descriptions for charge transfer kinetics produce a consistent model for series hopping transport through these films.

Experimental Methods

Materials

Polystyrene, PS, with narrow molecular weight distribution $M_w/M_n = \theta$ ($M_w = 61,800$ g mol-1, $M_n = 58,000$ g mol-1, $\theta = 1.07$) was obtained from Scientific Polymer Products. Poly (diallyldimethylammonium chloride) (PDADMAC, $M_w = 70,000$ g mol-1, $M_n = 61,600$ g mol-1, $\theta = 1.13$) and sodium polystyrene sulfonate NaPSS ($\theta = 120,000$ g mol-1, $\theta = 116,000$ g mol-1, $\theta = 1.03$) were prepared by fractionating broad $\theta = 120,000$ g mol-1, $\theta = 116,000$ g mol-1, $\theta = 116$

³⁵S-Labeled Sulfonation of PS

For the sulfonation procedure employed, a small particle size of starting PS is required. PS was reprecipitated as described previously with a slight modification. Briefly, 1 g of PS was dissolved in 100 mL MEK. 13 mL of methanol were added dropwise to the first sign of turbidity with vigorous stirring. This turbid mixture was added in a thin stream to 200 mL of methanol with vigorous stirring. After the powder settled for about 2 h, the supernate was decanted and the reprecipitated PS was washed 3x with methanol and dried under vacuum for 12 h. A fine white powder was obtained and sorted through a 106 µm sonic sifter sieve (Advantech Manufacturing).

In a capped scintillation vial, 0.4 mL of concentrated H_2SO_4 was added to 5 mCi of dry $Na_2^{35}SO_4$ and allowed to mix for 15 min. The sulfonation of PS powder was done according to the method of Coughlin *et al.* whereby 20 mg of fine PS was added to the labeled H_2SO_4 and placed in a preheated oil bath (90 °C) for 4 h (Scheme 1).³² The contents were mixed vigorously throughout the reaction and the vial was shaken every hour to dissolve the powder stuck to the walls. The reaction was quenched by pouring the mixture in 30 mL of cold water. The solution was neutralized with 1 M NaOH, then dialyzed against water using 3500 molecular weight cutoff dialysis tubing (SnakeSkin, Thermo Scientific) for two days.

The resulting mixture was filtered through a 0.1 μ m syringe filter (Acrodisc, PALL) and the absorbance was measured on a UV-vis spectrometer (Cary 100-Bio). The labeled PSS concentration was determined using the absorbance at λ = 225 nm and the extinction coefficient of PSS (See Supporting Information, Figure S1).

Scheme 1. Sulfonation of Polystyrene

PEMUs Buildup

PDADMA/PSS polyelectrolyte multilayers (PEMUs) were deposited directly onto the surface of platinum rotating disk electrode, RDE, of area 0.126 cm² which was polished with 0.3

µm alumina, sonicated for 15 s, rinsed with deionized water, and then dried under a stream of N_2 . Polyelectrolytes were built using layer-by-layer adsorption at room temperature with the aid of a robot (StratoSequence V, nanoStrata Inc.). The RDE was mounted to a shaft rotating at 150 rpm and alternately dipped for 10 min in polymer solutions (0.57 mM polyelectrolyte concentration, based on the concentration of the repeat unit, in 0.1 M NaCl) with three rinsing steps with 0.1 M NaCl (1 min each) in between. This cycle constitutes one bilayer and was repeated to generate films of 1-7 bilayers. Hence, the notation (PDADMA/PSS)_n refers to films, with "n" indicating the number of bilayers.

In similar experiments, films were built on a platinum sheet (0.1 mm thick, 2.5 cm wide, 5 cm long) treated in the same way as the RDE and on 1 x 1 inch double-side-polished silicon wafers (0.5 mm thick) that were cleaned by soaking them in $3:1 H_2SO_4:H_2O_2$ "piranha solution for 20 min, rinsing in deionized water and drying under a stream of N_2 .

Film Thickness

The backs of the substrates were cleaned with 2.5 M KBr, rinsed with deionized water and dried with N_2 to remove any polyelectrolyte complex. The thickness on Si wafers was determined using a Gaertner Scientific L116S autogain ellipsometer equipped with a 632.8 nm laser at a 70° incident angle, fixing the refractive index of the films at 1.54 and that of Si at 3.85.

The dry thickness on the Pt substrate for each bilayer was obtained by radiocounting. In a dark box the substrate was placed, face down, on an aluminum spacer with a 2 cm x 2 cm opening on top of a plastic scintillator disk (3.8 cm diameter, 3 mm thick, SCSN-81, Kuraray). The scintillator was placed on a photomultiplier tube (PMT, RCA 8850) connected to high voltage supply (Bertan 313B) at 2.3 kV, and a frequency counter (Philips PM6654C). To ensure good optical contact, a drop of immersion oil was placed between the PMT window and the scintillator disk. The scintillation counts were recorded using LabView software. Counting was performed for 15 min and the gate time and pulse threshold were fixed at 10 s and -20 mV respectively. A calibration curve was generated by dispensing 10 - 70 μ L of the labeled PSS solution under the substrate to translate the counts into mass of PSS per cm². The thickness was calculated assuming a density of 1.26 g cm³ for PDADMA/PSS complex³³ and a 4 cm² exposed area.

AFM imaging

An MFP-3D atomic force microscope (AFM, Asylum Research) equipped with an ARC2 controller and silicon TESPA-V2 probes (Bruker, radius = 10 nm, spring constant = 42 N m $^{-1}$) was used to evaluate the topography of the PEMUs. The intermittent contact or "AC mode" was selected, and the cantilever was tuned to 5% below its resonance frequency. A scan area of 1 x 1 μ m was used to obtain the roughness and to show the topology of PEMUs.

Electrochemistry

The current of $\text{Fe}(\text{CN})_6^{4-}$ redox ions through the PEMUs as a function of the number of layers was measured using cyclic voltammetry. The temperature in a 100 mL electrochemical cell was controlled at 25 °C (± 0.1 °C) using a water jacket and a circulating thermostat. A three-electrode system was adapted with a platinum wire counter electrode, a KCl-saturated calomel reference electrode (SCE) and a rotating platinum disk working electrode (RDE, 4 mm diameter) which was polished with 0.3 μ m alumina, sonicated for 15 s, rinsed with deionized water and dried under a stream of N_2 prior to the adsorption of polyelectrolytes onto its surface. The working electrode was mounted on a Pine Instruments AFMSRCE rotator with a speed controller and

potential ramps were generated using a Pine AFTP1 WaveNow potentiostat. All solutions were purged for 10 min with Ar and then blanketed with Ar to exclude O₂. The potential was swept at a scan rate of 10 mV s⁻¹ in the range -150 to 400 mV vs. SCE at 1000 rpm and the resulting voltammograms of 0.1 mM ferrocyanide solutions in 0.1 M NaCl were recorded using Aftermath software with 1 mV intervals between data points. Every 10 current readings were averaged, giving an interval of 10 mV between each data point. The experiment was performed under the same conditions in 0.1 M NaCl only to obtain background CVs. The rotation rate was not varied, which is often done in classical electron kinetics studies at the RDE, because vortexing of the solution under the electrode was observed for rpms greater than about 2000.

Diffusion of Ferro- and Ferricyanide

PEMUs were made on double side polished Si (100) wafers. For ferrocyanide diffusion measurements, multilayers were made with 10 mM polymer in 0.1 M NaCl, 5-minute dip times for each layer, with three, one-minute water rinses between layers, yielding a 32 nm thick film. Samples to measure the diffusion of sodium ferricyanide were made in a similar way, with 10 mM polymer in 1 M NaCl, 5 minute dip times with 3 one minute water rinses for each layer to give 99 nm films. Films were immersed in either 0.1 mM potassium ferrocyanide or 0.1 mM potassium ferricyanide in 0.1 M NaCl at room temperature, removed at fixed intervals, blown dry with a stream of nitrogen, and FTIR spectra were recorded at a resolution of 4 cm⁻¹. A standard of ferrocyanide complexed by PDADMA was prepared by mixing 10 mL of 10 mM PDADMA with 10 mL 5 mM potassium ferrocyanide (a 2-fold excess of ferrocyanide). The resulting complex, which had a 4:1 molar ratio of PDADMA:ferrocyanide, was washed with water and pressed against a diamond ATR crystal (Pike Inc.) to record infrared spectra. ATR spectra were corrected for comparison to transmission spectra using the OMNIC ATR correction feature.

Results and Discussion

Ultrathin multilayer films with thicknesses up to 15 nm were prepared on platinum to explore the effectiveness of PEMUs as barriers to electron transport. The pair of polyelectrolytes employed are well known in the PEMU literature: poly(styrene sulfonate), PSS, and poly(diallyl dimethylammonium chloride), PDADMAC. Here, both polymers had molecular weights to provide the same number of repeat units (about 600) and both had narrow molecular weight distributions, M_w/M_n (= θ). The multilayers were deposited under conditions known to provide stoichiometric films with low residual surface charge. On a macroscopic scale, such a composition has a glass transition temperature, T_g , when immersed in water, of about 35 °C. 34 It is believed that the T_g of ultrathin films may well be lower, but PDADMA/PSS films ca. 20 nm thick also provided a T_g of about 35 °C. 35 In any case, because it is electrons that are traversing the film and not ions, the T_g is not of prime importance here.

Electrochemical methods were used to assess the rate of electron transport as a function of film thickness. The rotating disc electrode (RDE) provides well-defined boundary conditions operating under steady-state.³⁶ Ferrocyanide was used as a solution redox species to provide electrons, since it cannot diffuse through the PEMU at a measurable rate under these conditions.³⁷ In their analysis of electron transfer kinetics, Feldberg and Sutin³⁸ emphasized the advantages of a steady-state current at microelectrodes, a geometry recently used by Velický et al. to explore tunneling through boron nitride, BN, films.³⁹ The RDE has recently been used by Sato et al. to study electron transfer to oxygen *via* catalysts tethered to gold electrodes.⁴⁰

The use of PEMUs on RDEs offers some additional potential benefits: first, the layer-by-layer addition of polymers, performed in ambient conditions, is rather "forgiving" of defects such as dust particles: each layer deposits over such defects. Second, the PEMU itself is amorphous and does not affect tunneling currents *via* phonons and crystal boundaries the way an inorganic layer such as BN or MgO might.

Thickness Measurements

The number of methods of performing accurate thickness measurements for organic films less than 10 nm on polished Pt surfaces is limited. Typically, the thickness of a multilayer is measured on a surrogate silicon wafer substrate using ellipsometry. While it is assumed and generally shown that the thicknesses of PEMUs grown under identical conditions on different substrates is the same, it is not known whether this trend holds for the first few nm on Pt metal.

An attempt made to acquire reflectance IR spectra at low angle using FTIR did not provide sufficient signal for an accurate measurement. Thus, a more involved, but accurate, route was taken: radiolabeled PSS was prepared using 35 S-labeled concentrated sulfuric acid. Sulfonation of polystyrene in conc. H_2SO_4 has been shown to provide 100% sulfonated material with no evidence of crosslinking. 32

PEMUs were built on a polished Pt sheet using 0.57 mM PSS (concentration based on the repeat unit and determined via UV-vis absorption, see Supporting Information Figure S1) in 0.1 M NaCl. After each bilayer, the film was rinsed and dried and 4 cm² of the PEMU was exposed through a mask to plastic scintillator. The counts collected for 15 min were converted to mass per cm² using a calibration curve (Figure S2, Supporting Information). The thickness, *d* (nm) of each bilayer was calculated using a PEMU density of 1.26 g cm⁻³ (see Supporting Information for an example).

For comparison, the thicknesses of PEMUs constructed under identical conditions on Si (100) were determined using ellipsometry. A "bilayer" is the term used for the thickness increment provided by the adsorption of a PDADMA and a PSS layer. In reality, the polyelectrolytes do not remain in layers and mix completely to yield a molecular blend.²⁶ If a PEMU is terminated with PDADMA the entire film contains excess PDADMA, which may allow partitioning of ferrocyanide into the films *via* Donnan inclusion. If the PEMU is terminated with PSS (up to about 14 layers), the film is stoichiometric in PDADMA and PSS and contains no ions.⁴¹ For this reason, measurements were made only with even numbers of layers.

Thickness *versus* layer number for the two techniques is reported in Figure 1. It is apparent that even multilayers less than 20 nm thick show the same buildup on the two different substrates. In agreement with the previously described mechanism,⁴¹ the assembly of PEMUs showed a "nonlinear" or a slightly curved buildup at the beginning on both substrates after which it became linear. A slight difference is observed only for the first few layers after which the influence of the substrate diminishes and the interaction between the polyelectrolytes solely controls the film buildup.

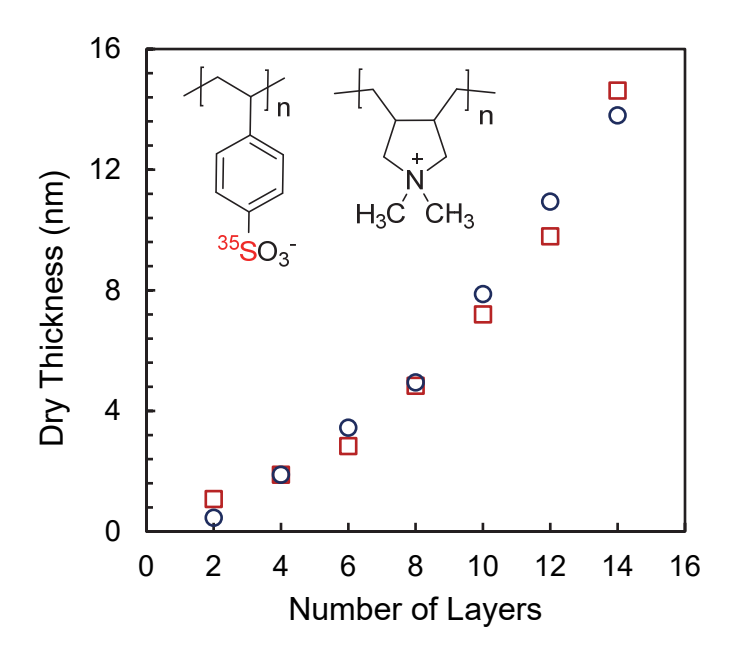


Figure 1. Dry thickness of PDADMA/PSS PEMU films *versus* number of layers built at 0.57 mM polymer concentration in 0.1 M NaCl on Pt sheet and measured using radiolabeling (open circles) or on Si wafer and measured using ellipsometry (open squares). Error is ±0.2 nm. Inset shows structures of PSS (left, labeled with ³⁵S) and PDADMA (right).

Topography

Scanning electron microscope images (Supporting Information Figure S3) showed the electrode to be relatively smooth but lacked the resolution to measure the nm roughness or thickness (Figure 1) of PEMUs. Thus, the topography and roughness of dry PEMU films built on Si wafers were obtained using atomic force microscopy (AFM). The AFM images in Figure 2 show PDADMA/PSS films are evenly deposited on the surface of the substrate. Certain combinations of polyelectrolytes are known to build "exponentially" when assembled layer-by-layer. Evidence for island-like growth or dewetting in sometimes observed. The PDADAMA/PSS pair interacts rather strongly and no evidence of defects such as phase separation, porosity, and dewetting can be observed from the AFM images in Figure 2 (the 2D images are shown in the Supporting Information Figure S4). The rms roughness of the films increases with film thickness as seen previously. To estimate the effective thickness of each multilayer representing the distance-of-closest approach to the electrode, half the rms roughness was subtracted from the thickness values of the films on Pt determined *via* radiolabeling. These results are summarized in Table 1.

Interestingly, the thickness and roughness of most multilayers were much less than the dimensions of the polymer coil in solution or within an equilibrated bulk complex of PDADMA/PSS. For example, PSSNa of similar molar mass in 0.05 M NaCl has a radius of gyration R_g of about 17 nm.⁴⁶ Within complexed bulk PDADMA/PSS, R_g for the PSS component is about 11.5 nm.⁴⁷ Up to 10 layers (~8 nm), the polymers must be adsorbed in a flattened conformation.

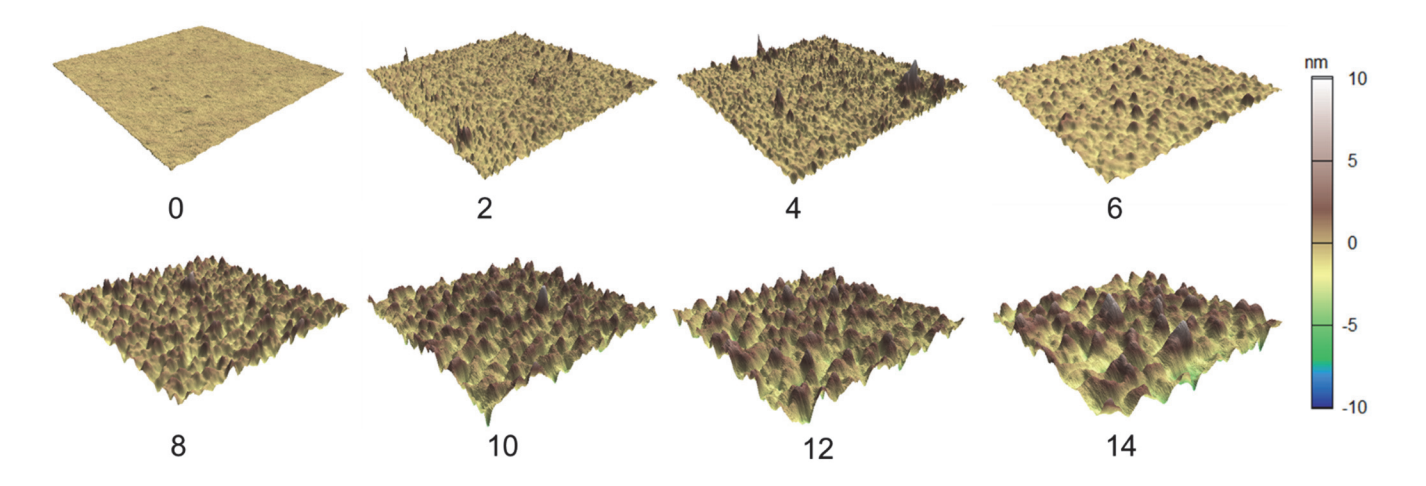


Figure 2. AFM images showing 3D topography of PDADMA/PSS films built on Si wafers in 0.1 M NaCl. The X-Y image area is 1 x 1 μ m. The number of layers is depicted under each representation. The rms roughness increases with the number of layers, given in Table 1.

 Table 1. PDADMA/PSS PEMU dry thickness measurements

Layer#	Dry Thickness on Pt (nm) ± 0.1 nm	^a Dry Thickness on Si (nm) ± 0.2 nm	^b Roughness dry (nm)	Effective Dry Thickness on Pt (nm)	^c Effective Wet Thickness on Pt (nm)
2	0.7	1.1	0.5	0.5	0.8
4	2.2	1.9	0.6	1.9	3.4
6	3.7	2.8	0.5	3.4	6.1
8	5.5	4.8	1.1	4.9	8.8
10	8.6	7.2	1.5	7.9	14.2
12	11.7	9.8	1.5	10.9	19.6
14	14.7	14.6	1.8	13.8	24.8

^aa 1.1 nm thick native oxide layer on the Si surface was subtracted.

^bThe rms roughness of the bare Si wafer was 0.2 nm

°wet thickness = 1.8 x dry thickness

PEMUs generally swell with water when placed in contact with aqueous solutions. The equilibrium water content of PDADMA/PSS in aqueous solutions of 0.1 M NaCl is known to be 40 ± 2 weight%.⁴⁸ Thus, all the dry thicknesses in Table 1 were multiplied by a factor of 1.8 to account for the water content (See Supporting Information for details). These wet thickness values (Table 1) were used to analyze electron transport data below.

Electron Transfer through Thin Films

PEMU films were built on the platinum rotating disc electrode, RDE, under conditions identical to those for Pt foil and Si wafer. The boundary conditions for convective transport to the RDE are precise and well described by theory. ³⁶ Because the electrode rotates, the current is at steady-state, which means the current at a particular voltage does not change with time, in contrast with static macroelectrodes. ³⁶ Electrons were transferred through the PEMU to the electrode from ferrocyanide in solution.

$$Fe(CN)_6^{4-} \to Fe(CN)_6^{3-} + e^-$$
 [1]

Cyclic voltammetry provided the current-voltage response. The ferri/ferrocyanide system has fast (reversible) electron transfer kinetics at the bare Pt electrode, which means the current at the bare electrode is limited only by convective-diffusion transport (Scheme 2A). The typical response is an "S"-shaped wave, shown in Figure 3, where the plateau or limiting current density $j_{l,rev}$ (A cm⁻²) at an electrode rotating at angular velocity ω (rad s⁻¹) is given by the Levich equation³⁶

$$j_{l,rev} = 0.62 \, nF D_s^{\frac{2}{3}} \omega^{\frac{1}{2}} v^{\frac{-1}{6}} C$$
 [2]

where n represents the number of electrons transferred (1 for ferrocyanide), F is Faraday's constant (96,490 C mol⁻¹), D_s is the solution diffusion coefficient (cm² s⁻¹), C is the solution concentration (mol cm⁻³), and v is the kinematic viscosity of the solution (cm² s⁻¹).

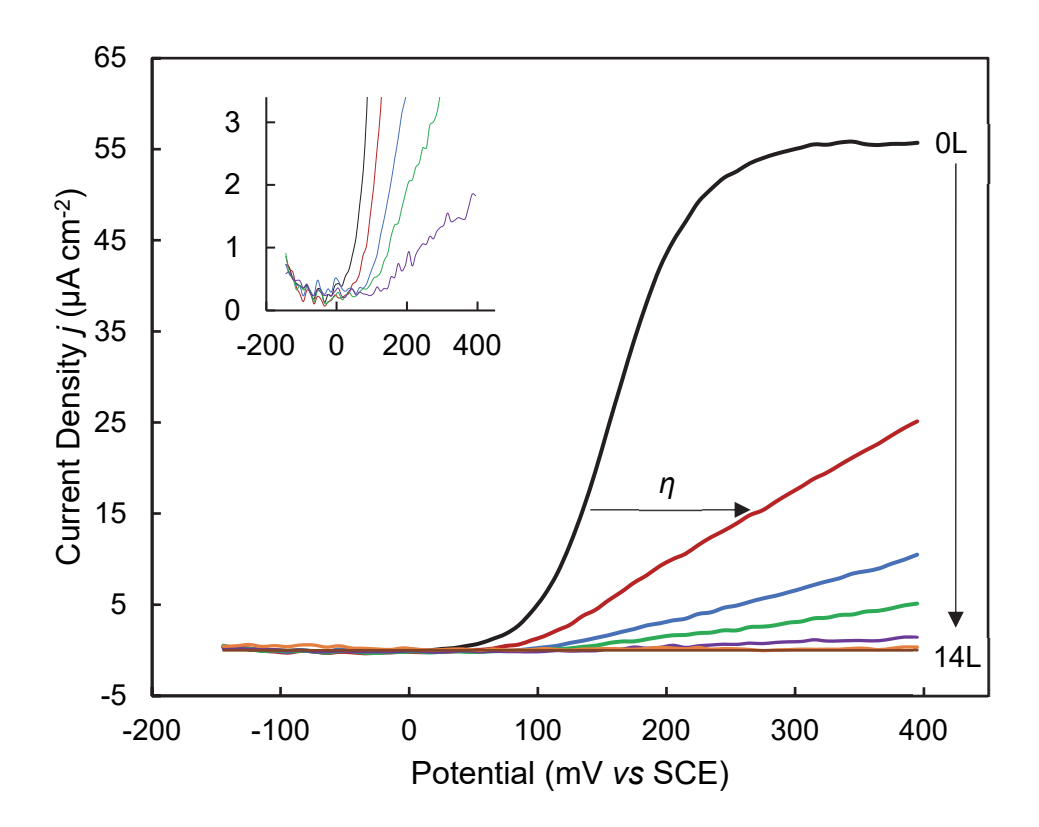


Figure 3. Voltammograms of 0.1 mM ferrocyanide in 0.1 M NaCl on PDADMA/PSS films at the Pt RDE. Electrode area = 0.126 cm², 25 °C, 10 mV s⁻¹ sweep rate, and 1000 rpm rotation rate. A background of each film in 0.1 M NaCl only was subtracted to remove the small charging current. The data average the forward and backward scans. η represents the overpotential. The inset shows an enlarged scale of the current density vs potential for the bare electrode and films of thickness 2-8 layers.

Current, j_{rev} , as a function of potential, E, for the reversible system, where the surface concentrations follow the Nernst equation (equilibrium), is given by

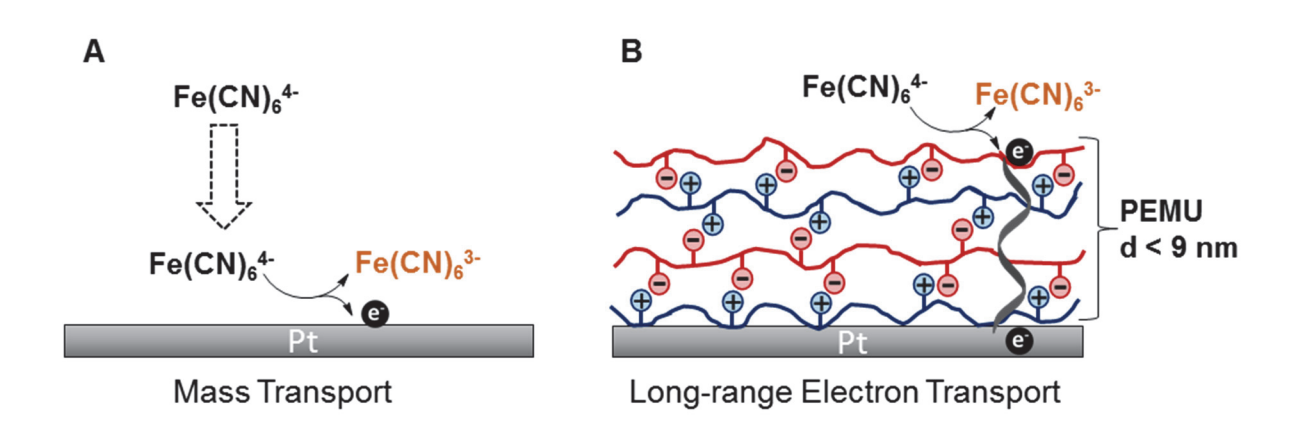
$$\frac{j_{rev}}{(j_{lrev} - j_{rev})} = e^{f(E - E_{1/2})}$$
 [3]

where f = nF/RT and $E_{1/2}$ is the half-wave potential. The voltammogram for the bare electrode is simulated using Equation 3 in Supporting Information Figure S6.

In systems where the electron transfer is further slowed by a film or other sources of poor transfer kinetics, the net current density j is expressed by the Koutecký-Levich equation³⁶

$$\frac{1}{j} = \frac{1}{j_K} + \frac{1}{j_{rev}} \tag{4}$$

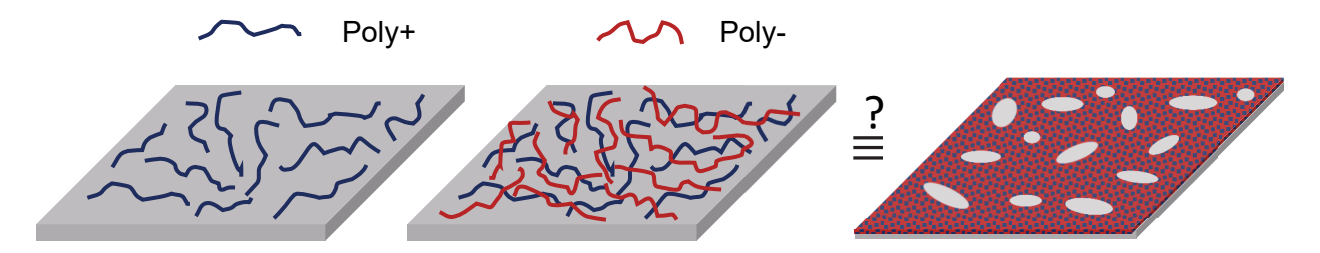
where j_K is the component of the current limited by sources other than solution mass transport. If the current is limited by diffusion of redox species through the film, the voltammogram remains S-shaped with a lower limiting current.^{49, 50, 51} In the present situation, the voltammogram loses its classical shape and has the appearance of a ramp, wherein j_k is a function of applied potential, and the net current is limited by electron transfer kinetics (Scheme 2B).



Scheme 2. Redox current at the electrode. A) Bare electrode with reversible (fast) electron transfer kinetics. Current is limited by convection and/or diffusion to the electrode surface (dotted arrows). B) Electrode covered with ultrathin film impermeable to Fe(CN)₆⁴⁻. The current is limited by slower electron transfer kinetics due to long-range transport (wavelike arrow). The PEMU is shown with stoichiometric, paired positive and negative polyelectrolyte units.

Figure 3 shows the current to the RDE is strongly attenuated by depositing ultrathin PEMU films on it. Even one bilayer produces a ramp-like current response and 12 layers reduces the signal to the level of the background. The shape of the wave indicates an electron-transfer limited current rather than a ferrocyanide-mass-transport limited current.

The shape of the redox wave also provides important information concerning the efficiency of the polymer film in producing a complete conformal coating. The cartoon in Scheme 2 illustrates polymer adsorption to a surface. Unlike self-assembled monolayers, such as those made from alkanethiols or silane-terminated small molecules, an adsorbed polymer chain is not expected to pack with crystalline order. Absorption of another "layer" of polyelectrolyte, here PSS, is shown in Scheme 2 to represent the thinnest PEMU film studied. A dry "bilayer" of PDADMA/PSS units, molar mass = 308 g mol⁻¹, density = 1.26 g cm⁻³, would be about 0.7 nm thick, or 1.3 nm when wet, which is approximately the value observed for the first bilayer. Despite this minimal thickness, the first bilayer provides efficient coverage, possibly due to efficient wetting of the Pt surface by the polymer. Larger area AFM scans show the presence of dust particles. Defects such as dust and pinholes may exist but are too few to influence the electrochemistry. A dense pinhole scenario, depicted in Scheme 3, may be discounted because dense pinholes would give voltammograms that exhibit either an S-shape or a peak depending on the spacing of the pinholes. ^{52, 53}



Scheme 3. Growth of polyelectrolyte multilayer on a surface using LBL adsorption. The panel on the right shows a representation of densely-spaced pinholes.

Current vs. Overpotential

In a reversible system, redox species at the electrode surface are maintained at their equilibrium concentrations as dictated by the Nernst equation. For slow electron transfer (irreversible system), additional voltage or overpotential is needed to drive electron transfer. The overpotential η for any current may be read from the graph as shown in Figure 3.

To extract j_K from the measured j using Equation 4, voltammograms on bare electrodes must be obtained (see Supporting Information Figure S6). Kinetic current versus overpotential plots of (even) layers 2 thru 8 are shown in Figure 4. The electron-transfer-kinetics-limited current density j_K as a function of overpotential η is typically described by the Butler-Volmer, BV, equation³⁶

$$j_K = -j_0 [e^{-\alpha f \eta} - e^{(1-\alpha)f \eta}]$$
 [5]

where j_0 is the exchange current density at zero overpotential, α is the anodic transfer coefficient and f is F/RT. In the present work, anodic current (oxidation) is defined as positive.

Plots of $\ln j_{K}$ versus η for PEMUs as a function of the number of layers were generated. Currents for layer numbers > 8 were noisy (Supporting Information Figure S6) and approached the background observed for electrolyte only (0.1 M NaCl without ferrocyanide). $\ln j_{K}$ versus η (Figure 4B) are linear beyond 50-200 mV overpotential with intercepts of j_{0} for each film.

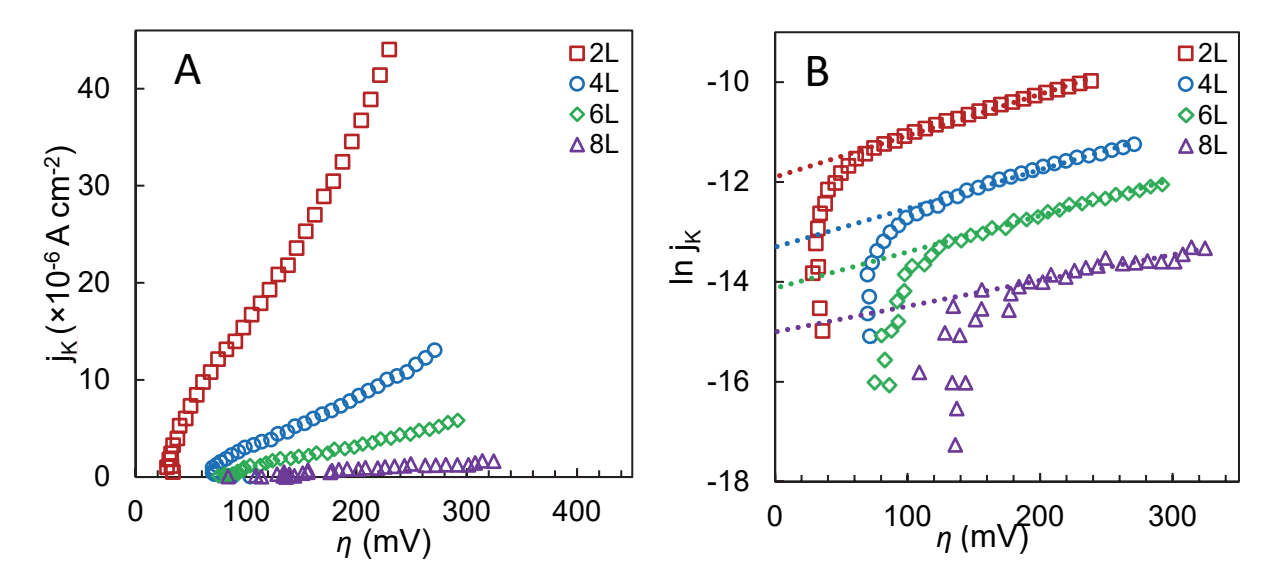


Figure 4. A. Kinetic current density, j_K versus overpotential for PEMUs with various numbers of layers for a 0.126 cm² Pt RDE at 25 °C using Equation 4 and data from Figure 3. **B.** Inj_K (j_K in A cm⁻²) as a function of overpotential for the first 4 bilayers. The intercepts on the j_K axis are j_0 . An apparent transfer coefficient, α , can be extracted from the slope of the curves.

Current vs thickness: Electron transfer Mechanisms

Electron transfer⁵⁴ occurs between a film-covered electrode and redox species, ^{1, 39, 55} two electrodes separated by an insulating spacer or molecule, ^{7, 15, 56} a donor and acceptor immobilized in a glass, ⁵⁷ or a donor and acceptor at opposite ends of a molecule. ^{13, 14, 17} In these scenarios, the dependence of transfer rate on distance is a commonly-sought parameter.

Table 1 shows that the length-scale resolution of the multilayer film system used here is 1 - 2 nm per bilayer, with the thinnest effective thickness about 1 nm for the first bilayer. With such a minimum thickness, the regime accessed by this multilayer is considered to be in the "long" range^{3, 14} of electron transfer. For "short" range electron tunneling, j commonly decays exponentially with increasing distance at a fixed applied potential

$$j = j_{0,b}e^{-\beta d} \tag{6}$$

where β is the rate of decay (nm⁻¹ or Å⁻¹) and $j_{0,b}$ is the maximum exchange current density, obtained when d=0 (i.e. a bare electrode). Note that the exponential falloff of current with distance in Equation 6 is used even if the system is beyond the "short" (tunneling) range. For reference, the value of $j_{0,b}=0.019$ A cm⁻² using a value of about 2 cm s⁻¹ for the heterogeneous rate constant k° of ferri/ferrocyanide at a clean bare electrode,⁵⁸ is also given on Figure 5 ($j_0=Fk^{\circ}C$). Using the j values from the intercepts in Figure 4B provides a β of 10 nm⁻¹ for d < 1 nm (short range) and an apparent β of 0.35 nm⁻¹ over the range 1 - 9 nm actually studied in the present work. The initial β should be considered a lower limit, as the falloff may be steeper. The change in slope (10 nm⁻¹ to 0.35 nm⁻¹) indicates that the mechanism changes at a thickness of about 1 nm, or, more precisely, from bare to a coated electrode. These two slopes yield two intercepts: $j_{0,b}$ for the bare electrode and $j_{0,film}$ for the multilayer covered electrode.

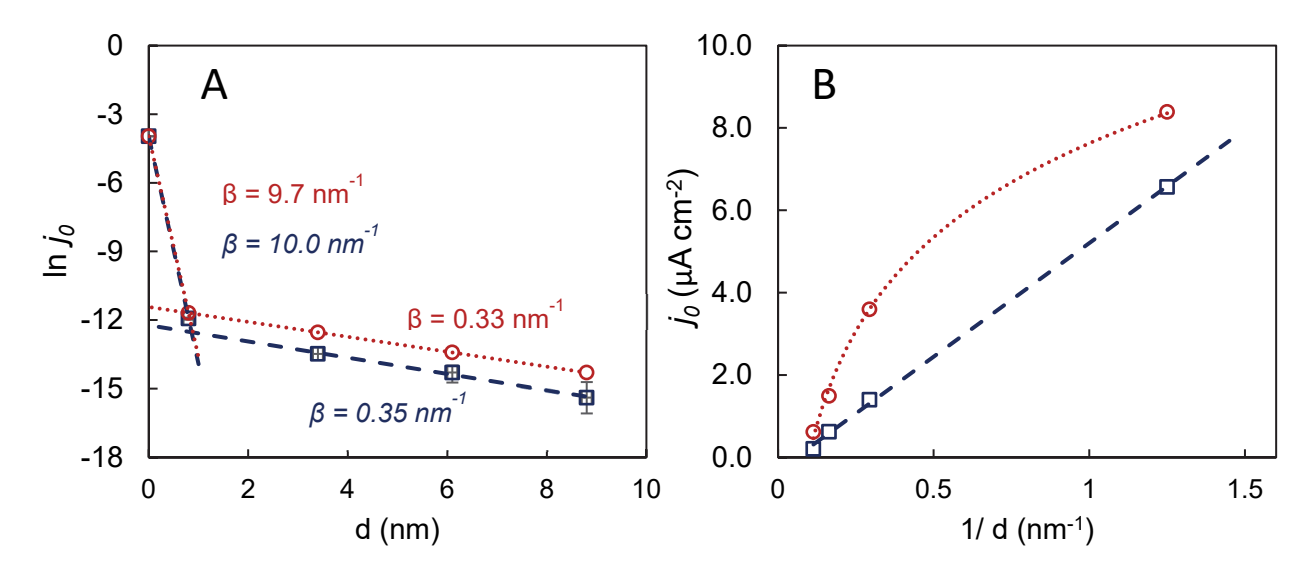


Figure 5. A. *Ln* of the exchange current density j_0 (A cm⁻²) as a function of PEMU thickness along with β values for < 1 nm and > 1 nm thickness using *apparent* values (open squares, dashed lines, italic font) and *fit* values from Equation 16 (open circles, dotted lines). Apparent values were taken directly from Figure 4 assuming no intermediate hopping steps, whereas fit values assume there is hopping within the film. **B.** j_0 versus 1/thickness using the same data. For **A**, Intercept $j_{0,b}$ for the bare electrode is 0.019 A cm⁻² and intercept $j_{0,film}$ for the coated electrode is 4.9 μA cm⁻².

Changes in β are often observed as a function of d. For example, Velický et al. have recently studied tunneling though microdisks of hexagonal boron nitride film, HBN, separating graphite electrodes from solution redox species.³⁹ A change in β from ~11 nm⁻¹ to ~2 nm⁻¹ was observed at an HBN thickness of around 0.7 nm. Yan et al.⁵⁹ observed three distinct regions in β (2.9 nm⁻¹, 0.8 nm⁻¹, 0.015 nm⁻¹) for electron transport across bis-thienylbenzene films of thickness 4 to 22 nm.

All data for the PEMU-covered electrodes fall close to the β = 0.3 nm⁻¹ line (Figure 5), which suggests hopping transport among states. Transport over the d range in Figure 5 with a small β is often found in conjugated molecular wires, although the conjugation is believed to support a tunneling mechanism up to ~5 nm. Sedghi et al.¹⁵ and Kuang et al.²⁹ claim on-resonance tunneling can be operative in oligoporphyrin spacers with a β = 0.4 nm.²⁹

In some treatments of hopping models, current is predicted to be proportional to 1/d, 60 in apparent agreement with the data here (see Figure 5B). The composition of a PEMU is unlike that of most other media used to explore electron transfer: multilayers are ionic, well hydrated, full of aromatic groups, and bathed in mobile ions. In these respects, PEMUs most closely resemble DNA, which has an extensive history as a rodlike molecule use to explore electron transfer. Wohlgamuth et al. found an apparent β of 0.15 nm⁻¹ for a redox species interrogated electrochemically though DNA, 61 close to an upper limit of 0.5 nm⁻¹ found by Slinker et al. for a 34 nm strand of redox-tagged DNA. Tunneling through water has a low β (1.25 nm⁻¹ up to 2 nm). 62

Single-step tunneling transfer has been interpreted using adaptations of classical Marcus-Hush theory. 1 39 Feldberg and Sutin 38 provided an expression for calculating the formal rate constant k_b at a bare electrode for a nonadiabatic system (common for outer-sphere like ferrocyanide)

$$k_b^0 = \frac{2\pi^2 \rho_M [H_{12}^0]^2}{\beta h \sqrt{1 + \frac{\lambda}{\pi k_B T}}} e^{-\lambda/4k_B T}$$
 [7]

where λ is the reorganization energy (about 1 eV for ferri/ferrocyanide⁵⁵), k_B is Boltzmann's constant = 8.62 x10⁻⁵ eV K⁻¹, h is Planck's constant (= 4.16 x 10⁻¹⁵ eV s), ρ_M is the density of states (about 2.3 eV⁻¹ atom⁻¹ for platinum⁶³), $[H_{12}^0]$ is the electronic coupling element when d=0 (assumed to be about 0.1 eV here³⁸), T is the temperature. The calculated k^o for a bare Pt electrode is about 18 cm s⁻¹, which is higher than the 2 cm s⁻¹ determined for the "true" value of k^o for ferri/ferrocyanide on Pt.⁵⁸ If 2 cm s⁻¹ is the actual k^o , $[H_{12}^0]$ may be overestimated and is probably closer to 0.03 eV. In addition, Gosavi and Marcus⁶³ pointed out that a ρ_M of 2.2 for Pt may be significantly overestimated, since d orbitals are not strongly coupled to the environment.

Equation 7 was modified by Velický et al. to account for the distance dependence represented in Equation 6. i.e. multiplying by a factor $e^{-\beta d}$. Reasonable predictions were made for this tunneling model for HBN films, a β of about 11 nm⁻¹, and two redox species up to 0.7 nm, after which β decreased significantly. In the present case, Equation 7 does not predict the data in Figure 5A because the intercept k_b^0 is too small when extrapolating points beyond the first bilayer.

Nonconforming Behavior in Electron Transfer

In addition to the change in slope, there are a couple of odd features regarding the electron transfer data of Figure 4. First, *In* current/overpotential curves, known as Tafel plots, which adhere to the standard Butler-Volmer treatment should become linear after about 50 mV of overpotential.³⁶ Instead, Figure 4 shows the breakpoint between nonlinear and linear behavior shifts to steadily greater overpotential with thicker films.

Second, the transfer coefficients α , obtained from the slope of Figure 4 (using Equation 5), are unusually large (1- α unusually small, see Figure 6), and 1- α decreases with increasing thickness, an inconsistency noted by Velický et al.³⁹

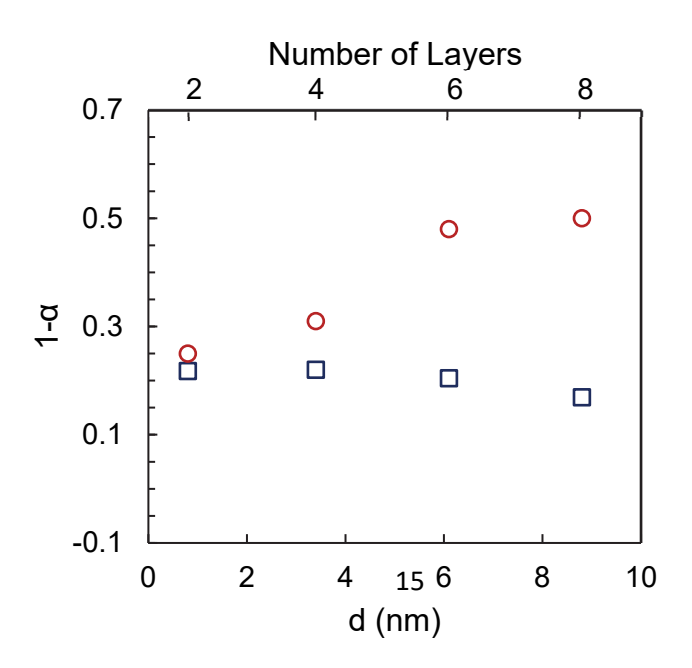


Figure 6. Dependence of the apparent transfer coefficient (open squares, from the slopes in Figure 4B) and transfer coefficient from fits to modified Butler-Volmer equation 18 (open circles) as a function of the PDADMA/PSS PEMU thickness for 0.1 mM ferrocyanide in 0.1 M NaCl for a 0.126 cm² Pt RDE at 25 °C.

Hopping Transport: Number of Hops

To reconcile these unusual features, a hopping model is proposed wherein the overpotential is distributed among hopping events, represented in Figure 7. Each hop is equivalent, except for the hop from film to electrode and the hop from solution redox species to film. Each hop may be considered a tunneling event. If the film is thin enough (less than 1 nm), coupling elements, density of states and reorganization energies in Equation 7 are, as discussed above, from bare metal to redox species with a β of about 10 nm⁻¹. For each hop that starts and ends within the film, the values of ρ and $[H_{12}]$ are not known but their product is much less than that at the bare metal, illustrated by the $j_{O,film}$ intercept that is orders of magnitude lower than $j_{O,b}$ on bare Pt. The "staircase" of intermediate energy levels is similar to that described by Renaud et al.⁶⁴ for hopping via DNA base pairs.

With hopping *via* charge-neutral DNA bases, which contain no discrete redox sites, the nature of charge localization is unclear. For DNA, it has been argued that hole density can be delocalized over several bases.⁶⁵⁶⁶

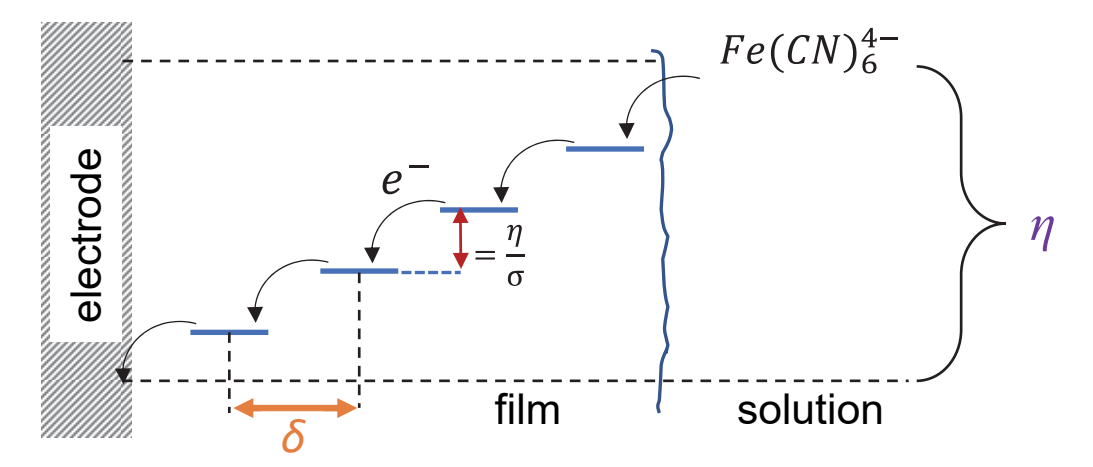


Figure 7. Model for hopping transport through an ultrathin film with electron transfer from ferrocyanide to the electrode with a total overpotential η . In this case, η is divided amongst σ hops through the film, separated by an average hopping range δ , which decreases the driving force for each hop to η/σ volts.

In the present case, discrete redox sites are provided by a population of ferrocyanide ions within the PEMU. To determine the concentration and rate of diffusion of ferrocyanide in the film, PEMUs were deposited on double-side-polished silicon wafers and immersed in 0.1 mM ferrocyanide in 0.1 M NaCl. The accumulation of ferrocyanide as a function of time was monitored by transmission FTIR using the strong CN stretching mode at about 2100 cm⁻¹ (see Supporting Information Figure S7). Figure 8 illustrates doping of a 32 nm film with ferrocyanide as a function of time^{1/2}.

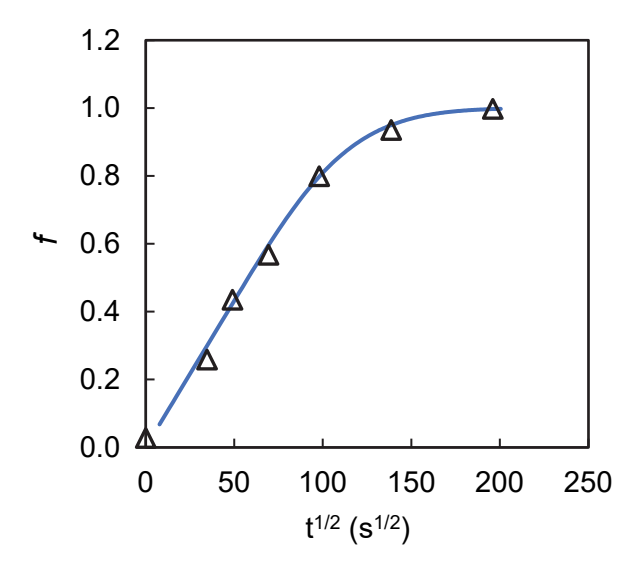


Figure 8. Room temperature doping of a 32 nm PDADMA/PSS PEMU as a function of time from 0.1 mM ferrocyanide in 0.1 M NaCl. The solid line is a fit to equation 8 with a D_f of 6 x 10^{-16} cm² s⁻¹. The equilibrium concentration of ferrocyanide in the PEMU is 0.032 M, which represents a 300-fold concentration of ferrocyanide from solution into the film.

The doping versus time was modeled using an equation for diffusion into one side of a plate under finite boundary conditions:⁶⁷

$$f = 1 - \sum_{n=0}^{\infty} \frac{8}{(2n+1)^2 \pi^2} \exp\left[\frac{-D_f (2n+1)^2 \pi^2 t}{4l^2}\right]$$
 [8]

where f is the fractional attainment of equilibrium concentration within the film, D_f is the film diffusion coefficient, t is time in seconds, l is the thickness of the film in cm, and n is an integer. The fit to the data in Figure 8 returns a value of 6 x 10^{-16} cm² s⁻¹ for diffusion of ferrocyanide in the PEMU at room temperature. This exceedingly low diffusion coefficient would nevertheless allow equilibration of a 10 nm film with ferrocyanide in about 10 minutes. Ball and Duval found similarly ultraslow diffusion of ferrocyanide in PDADMA/poly(acrylic acid) multilayers. ⁶⁸

The actual concentration of ferrocyanide in the film was measured by comparison with a standard of PDADMA precipitated in excess ferrocyanide washed with water and dried. The PEMU concentration of ferrocyanide, \bar{c} , was estimated to be 0.032 M (see Supporting Information for a full description), which translates to an average distance between ferrocyanide ions in the PEMU of 3.7 nm. The diffusion experiment was repeated with 0.1 mM sodium ferricyanide (3-charge) in 0.1 M NaCl using a 99 nm film, which came to an equilibrium PEMU concentration of 0.0024 M much faster, with a diffusion coefficient of 7 x 10⁻¹³ cm² s⁻¹ (Supporting Information Figure S8). The steady-state current density expected for PEMU diffusion-limited transport of ferrocyanide is

$$j = \frac{FD_f\bar{C}}{d} \tag{9}$$

Assuming a 10 nm thick film and inserting the known values returns a j of about 2×10^{-9} A cm⁻², which is three orders of magnitude less than the current actually seen – further evidence that electron transfer to the electrode by diffusion through the PEMU is negligible. The term "hopping range" is used below to indicate the distance that most (e.g. 95%) of hops take.

If the hopping range is δ nm, the number of hops to traverse a film of thickness d is

$$\sigma = 1 + d/\delta \tag{10}$$

(it takes at least one hop even if $d \ll \delta$).

The effect of carving up potential among hops is to decrease the overall driving force for each hop, thus current decreases. Assuming all hops to be equivalent, the BV equation is simply modified by decreasing the overpotential by a factor σ

$$j_K = -j_{0,\sigma} \left[e^{-\alpha f \eta/\sigma} - e^{(1-\alpha)f\eta/\sigma} \right]$$
 [11]

 $j_{0,\sigma}$ exponentially decays with the number of hops

$$j_{0,\sigma} = j_{0,film}e^{-\beta d} \tag{12}$$

Which is the familiar relationship of current (rate) *versus* distance. $j_{0,film}$ is the intercept at d = 0 (see Figure 5). Thus,

$$j_K = -j_{0,film} e^{-\beta d} \left[e^{-\alpha f \eta/\sigma} - e^{(1-\alpha)f\eta/\sigma} \right]$$
 [13]

For $\eta/\sigma > 50$ mV (at room temp) assuming $\alpha = 0.5$

$$j_K = j_{0,film} e^{\frac{0.5f\eta\delta}{d} - \beta d}$$
 [14]

For $\eta/\sigma < 50 \text{ mV}$

$$j_K = j_{0,film} f \frac{\eta}{1+\beta d} e^{-\beta d}$$
 [15]

The Meaning of β

The distance dependence of j_0 reflects the *number of hops* required to traverse the film.

$$j_{0,\sigma} = j_{0,film}e^{-(\sigma-1)}$$
 [16]

Thus, σ - 1 = βd and, using Equation 9

$$\beta = \frac{1}{\delta} \tag{17}$$

This very simple relationship may now be illustrated with the current data. Equations 12 and 16 provide $\sigma = 1 + \beta d$. In the present case, β is 0.326 nm⁻¹ and the hopping range is 3.07

nm, close to the value determined from the direct measurement of ferrocyanide above. Combining Equations 11 and 16

$$j_K = -j_{0,film}e^{-(\sigma-1)}[e^{-\alpha f\eta/\sigma} - e^{(1-\alpha)f\eta/\sigma}]$$
 [18]

Using Equation 18 and values of β = 0.326 nm⁻¹, the data from Figure 4 are replotted in Figure 9. The curves now converge as $\eta \rightarrow 0$ and approach linearity for value of $\eta/\sigma > 50$ mV. The only freely adjustable fit parameter is α , which turns out to reassuringly approach 0.5. The parameters used for the fit are provided in Table 2. After the subtraction of 20 mV from each experimental curve, attributed to the asymmetry of the first electron transfer, the simulated current-voltage curve reproduces the experimental well.

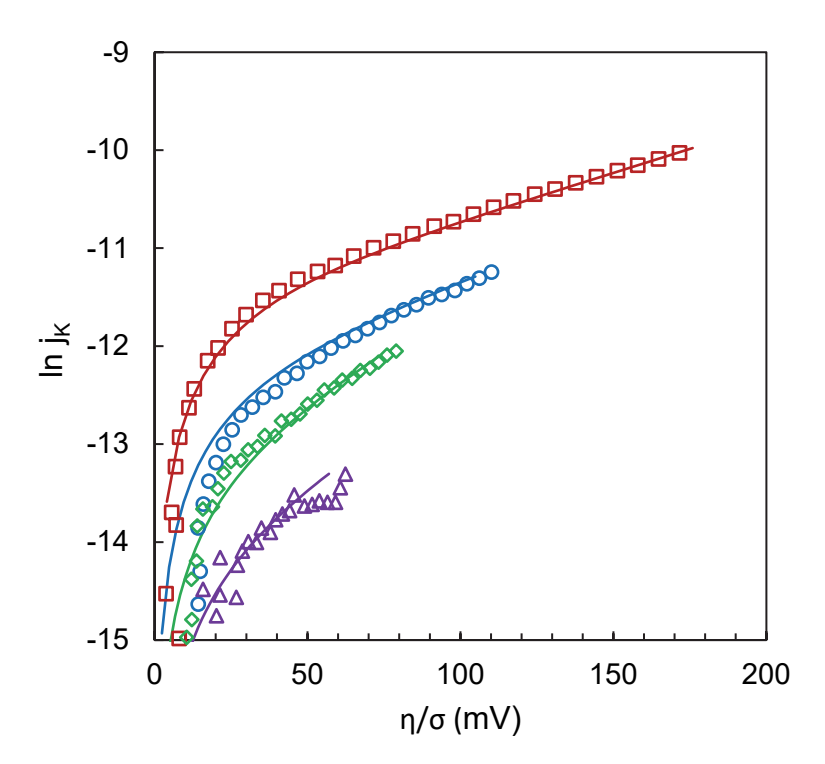


Figure 9. Ln of j_K (A cm⁻²) as function of η/σ (mV) for the first 4 PDADMA/PSS bilayers. 2 layers, squares; 4 layers, circles; 6 layers, diamonds; 8 layers, triangles. The solid lines are Equation 11 with parameters listed in Table 2. Room temperature is assumed where f = 38.9. The fit reproduces both the potential and the distance dependence of j_K .

Table 2. Values used in Equation 11

Layer#	Exchange Current Density ^a j _{0,σ} (μA cm ⁻²)	^b Transfer Coefficient α	^c Number of Hops σ
--------	--	---	----------------------------------

2	8.4	0.75	1.3
4	3.6	0.69	2.1
6	1.5	0.52	3.0
8	0.62	0.50	3.9

acalculated from eq 16

As the film thickness increases, the best-fit values for α now approach 0.5, which is expected for electron transfer between two identical systems (ferrocyanide ions; the best fit values for α are compared with the apparent values in Figure 6). The dependence of current on distance according to Equation 18 follows neither $j_K \sim e^{-\beta}$ nor $j_K \sim 1/d$ for all values of d. The dependence does, however, approximate $j_K \sim e^{-\beta}$ for moderate applied voltages and for d > 1 nm, illustrated by the simulation shown in Figure 10. This shows the importance of defining both the applied potential and the distance in each measurement to obtain mechanistic insight.

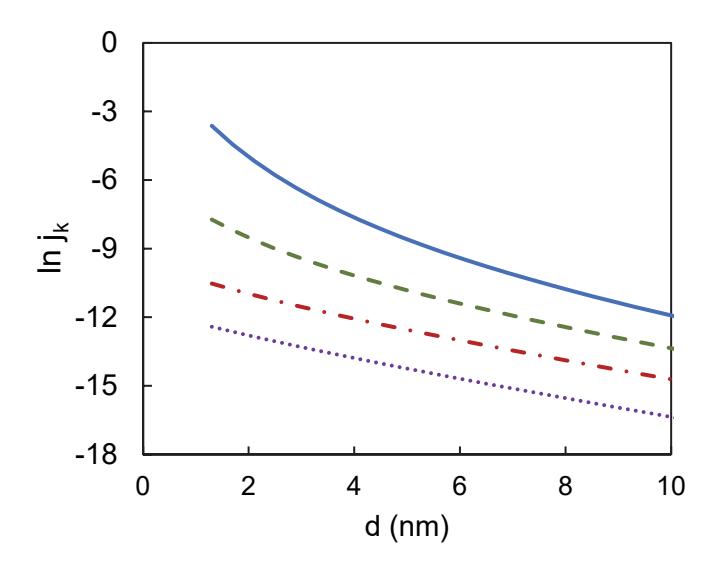


Figure 10. Simulation of j_k versus distance d for various applied potentials using the hopping model of Equation 18, $\sigma = 1 + \beta d$, $\beta = 0.326$ nm⁻¹ and lnj_{o,film} = -11.4. Applied potential = 20 mV (dotted line); 100 mV (dash-dot); 300 mV (dashed line); 600 mV (solid line). 25 °C.

badjusted to obtain best fit

 $^{^{\}circ}$ #hops = 1 + 0.326d

Michaeli et al.³⁰ have recently performed a theory analysis of long-range coherent electron transfer. They also break transport down into multistep hopping between sites and find, for a fixed voltage, there is an exponential decay of electron transmission with length for a sufficiently large number of sites.³⁰

Assumptions.

For the sake of simplicity, certain assumptions have been made, including the assumption that all hops are equal. The first hop is clearly different, occurring between metal and film. In fact, this is the transfer typically seen for short range. The influence of the first hop is to bias the coefficient α , which is a measure of the symmetry of the barrier for forward and backwards electron transfer. α quickly transitions to a value of 0.5 for thicker films (Figure 6), expected for hops between equivalent sites. The electron transfer distances (i.e. film thicknesses) probed in the current experiment, even for the first bilayer, are beyond the 1-step tunneling range from electrode to redox species. Experiments with greater distance resolution show the transition from tunneling to hopping more clearly. Examples of these experiments indicate the breakpoints in β between electron transfer regimes depends on the system. For nonconjugated systems the transition occurs at about 1 nm, 39 whereas for conjugated systems it is closer to 4 nm. 8 , 59 , 69

Other Systems

The concepts and comparisons of tunneling *versus* hopping are used extensively for diverse systems used to probe electron transfer. As occasionally pointed out, there are sure to be differences in behavior between electron transfer, for example in proteins versus DNA⁷⁰ and in general.⁸ The electrochemical system employed here is best compared with numerous studies employing electrochemistry, including many involving DNA. Electrochemistry allows the user to dial in the "driving force" (overpotential) for electron transfer without concern for the effect of contact resistance or contact properties encountered in "molecular wire" devices. The use of a uniform thin film avoids possible interference by a "tethering layer" such as an alkane thiol.²⁸

The simple inverse relationship of β to hopping range (Equation 17) implies conjugated molecular systems, with low values of β , β , β have long hopping ranges. This is made possible by the delocalization of π electrons over several carbons. For example, electrons in polyacetylene are distributed over a distance of about 15 C-C bonds or about 1.9 nm, which makes the maximum value of β about 0.5 nm one might expect a β -value of 3 nm are separated by a distance of about 0.33 nm one might expect a β -value of 3 nm hole dynamics in DNA led to the conclusion that, for DNA of intermediate length, delocalization of charge occurred over the entire system, β which would increase the effective hopping range considerably.

Conclusions

The thinnest possible film of complexed polyelectrolytes was made from a single bilayer of PDADMA and PSS. Though on the order of 1 nm thick, this film provides significant resistance to electron transfer from ferrocyanide in solution to an electrode. Beyond six additional layers (9 nm) the electrochemical current falls to the background level. Within the range of 1 - 9 nm corresponding to reliably measurable current, steady state voltammetry provides accurate measurements for the current-voltage response. The relatively weak distance dependence of current on electron transfer distance strongly suggests the current is limited by hopping. Using a

hopping model, overpotential in the classical Butler-Volmer equation may be partitioned over a number of equivalent hops. The derived expression fit the experimental data, where the hopping range was obtained from the falloff of rate versus distance, and the electron transfer coefficient α was selected to provide the best fit.

The system studied here provides an equilibrium population of virtually immobile ferrocyanide ions, between which electron hopping is possible. Other systems assumed to exhibit electron hopping transfer have less defined intermediate redox sites. Because β is inversely related to d in the hopping model, low values of β are consistent with charge that can be delocalized over a π -electron system, as found in conjugated polymers, or distortions that can be spread over more than one repeat unit (polarons).

Associated Content

Supporting Information

Calibration curves for thickness determination; simulation of reversible cyclic voltammetry; additional AFM images; cyclic voltammetry showing forward and reverse scans. The Supporting Information is available free of charge.

Author Information

Corresponding Author

*jschlenoff@fsu.edu

ORCID https://orcid.org/0000-0003-3258-5341

Notes

The authors declare no competing financial interests.

Acknowledgments

This work was supported by a grant from the National Science Foundation (DMR-1809304).

References

- 1. Chidsey, C. E. D. Free Energy and Temperature Dependence of Electron Transfer at the Metal-Electrolyte Interface. *Science* **1991**, *251*, 919-922.
- 2. Smalley, J. F.; Finklea, H. O.; Chidsey, C. E. D.; Linford, M. R.; Creager, S. E.; Ferraris, J. P.; Chalfant, K.; Zawodzinsk, T.; Feldberg, S. W.; Newton, M. D. Heterogeneous Electron-Transfer Kinetics

for Ruthenium and Ferrocene Redox Moieties through Alkanethiol Monolayers on Gold. *Journal of the American Chemical Society* **2003**, *125*, 2004-2013.

- 3. Genereux, J. C.; Barton, J. K. Mechanisms for DNA Charge Transport. *Chemical Reviews* **2010**, *110*, 1642-1662.
- 4. Miller, C.; Cuendet, P.; Graetzel, M. Adsorbed Omega-Hydroxy Thiol Monolayers on Gold Electrodes: Evidence for Electron Tunneling to Redox Species in Solution. *The Journal of Physical Chemistry* **1991**, *95*, 877-886.
- 5. Eckermann, A. L.; Feld, D. J.; Shaw, J. A.; Meade, T. J. Electrochemistry of Redox-Active Self-Assembled Monolayers. *Coordination Chemistry Reviews* **2010**, *254*, 1769-1802.
- 6. Finklea, H. O.; Hanshew, D. D. Electron-Transfer Kinetics in Organized Thiol Monolayers with Attached Pentaammine(Pyridine)Ruthenium Redox Centers. *Journal of the American Chemical Society* **1992,** *114*, 3173-3181.
- 7. Akkerman, H. B.; de Boer, B. Electrical Conduction through Single Molecules and Self-Assembled Monolayers. *Journal of Physics: Condensed Matter* **2007**, *20*, 013001.
- 8. Luo, L.; Choi, S. H.; Frisbie, C. D. Probing Hopping Conduction in Conjugated Molecular Wires Connected to Metal Electrodes. *Chemistry of Materials* **2011**, *23*, 631-645.
- 9. Cui, X. D.; Zarate, X.; Tomfohr, J.; Sankey, O. F.; Primak, A.; Moore, A. L.; Moore, T. A.; Gust, D.; Harris, G.; Lindsay, S. M. Making Electrical Contacts to Molecular Monolayers. *Nanotechnology* **2001**, *13*, 5-14.
- 10. Nitzan, A. Electron Transmission through Molecules and Molecular Interfaces. *Annual Review of Physical Chemistry* **2001**, *52*, 681-750.
- 11. McConnell, H. M. Intramolecular Charge Transfer in Aromatic Free Radicals. *The Journal of Chemical Physics* **1961**, *35*, 508-515.
- 12. He, J.; Chen, F.; Li, J.; Sankey, O. F.; Terazono, Y.; Herrero, C.; Gust, D.; Moore, T. A.; Moore, A. L.; Lindsay, S. M. Electronic Decay Constant of Carotenoid Polyenes from Single-Molecule Measurements. *Journal of the American Chemical Society* **2005**, *127*, 1384-1385.
- 13. Giacalone, F.; Segura, J. L.; Martín, N.; Guldi, D. M. Exceptionally Small Attenuation Factors in Molecular Wires. *Journal of the American Chemical Society* **2004**, *126*, 5340-5341.
- 14. Gilbert Gatty, M.; Kahnt, A.; Esdaile, L. J.; Hutin, M.; Anderson, H. L.; Albinsson, B. Hopping Versus Tunneling Mechanism for Long-Range Electron Transfer in Porphyrin Oligomer Bridged Donor–Acceptor Systems. *The Journal of Physical Chemistry B* **2015**, *119*, 7598-7611.
- 15. Sedghi, G.; García-Suárez, V. M.; Esdaile, L. J.; Anderson, H. L.; Lambert, C. J.; Martín, S.; Bethell, D.; Higgins, S. J.; Elliott, M.; Bennett, N. et al. Long-Range Electron Tunnelling in Oligo-Porphyrin Molecular Wires. *Nat Nanotechnol* **2011**, *6*, 517-523.
- 16. Zhang, Y.; Soni, S.; Krijger, T. L.; Gordiichuk, P.; Qiu, X.; Ye, G.; Jonkman, H. T.; Herrmann, A.; Zojer, K.; Zojer, E. et al. Tunneling Probability Increases with Distance in Junctions Comprising Self-Assembled Monolayers of Oligothiophenes. *Journal of the American Chemical Society* **2018**, *140*, 15048-15055.
- 17. Sukegawa, J.; Schubert, C.; Zhu, X.; Tsuji, H.; Guldi, D. M.; Nakamura, E. Electron Transfer through Rigid Organic Molecular Wires Enhanced by Electronic and Electron–Vibration Coupling. *Nat Chem* **2014**, *6*, 899-905.
- 18. Gilbert, M.; Albinsson, B. Photoinduced Charge and Energy Transfer in Molecular Wires. *Chem Soc Rev* **2015**, *44*, 845-862.
- 19. Giese, B. Long-Distance Charge Transport in DNA: The Hopping Mechanism. *Accounts of Chemical Research* **2000**, *33*, 631-636.
- 20. McDowell, M.; Hill, I. G.; McDermott, J. E.; Bernasek, S. L.; Schwartz, J. Improved Organic Thin-Film Transistor Performance Using Novel Self-Assembled Monolayers. *Applied Physics Letters* **2006**, *88*, 073505.

- 21. Boubour, E.; Lennox, R. B. Insulating Properties of Self-Assembled Monolayers Monitored by Impedance Spectroscopy. *Langmuir* **2000**, *16*, 4222-4228.
- Baumann, S.; Rau, I. G.; Loth, S.; Lutz, C. P.; Heinrich, A. J. Measuring the Three-Dimensional Structure of Ultrathin Insulating Films at the Atomic Scale. *ACS Nano* **2014**, *8*, 1739-1744.
- 23. Moon, H.; Seong, H.; Shin, W. C.; Park, W.-T.; Kim, M.; Lee, S.; Bong, J. H.; Noh, Y.-Y.; Cho, B. J.; Yoo, S.; et al. Synthesis of Ultrathin Polymer Insulating Layers by Initiated Chemical Vapour Deposition for Low-Power Soft Electronics. *Nature Materials* **2015**, *14*, 628-635.
- 24. Lihter, M.; Graf, M.; Iveković, D.; Radenovic, A. Nanoscale Selective Passivation of Electrodes Contacting a 2D Semiconductor. *Advanced Functional Materials* **2020**, *30*, 1907860.
- 25. McCarley, R. L.; Thomas, R. E.; Irene, E. A.; Murray, R. W. Optical, Electrical, and Electrochemical Characteristics of Ultrathin Poly(Phenylene Oxide) Films: Organic Dielectrics Less Than 10 nm Thick. *Journal of Electroanalytical Chemistry and Interfacial Electrochemistry* **1990**, *290*, 79-92.
- 26. Decher, G. Fuzzy Nanoassemblies: Toward Layered Polymeric Multicomposites. *Science* **1997**, 277, 1232-1237.
- 27. Bucur, C. B.; Sui, Z.; Schlenoff, J. B. Ideal Mixing in Polyelectrolyte Complexes and Multilayers: Entropy Driven Assembly. *Journal of the American Chemical Society* **2006**, *128*, 13690-13691.
- 28. Slinker, J. D.; Muren, N. B.; Renfrew, S. E.; Barton, J. K. DNA Charge Transport over 34 nm. *Nat Chem* **2011**, *3*, 228-233.
- 29. Kuang, G.; Chen, S.-Z.; Wang, W.; Lin, T.; Chen, K.; Shang, X.; Liu, P. N.; Lin, N. Resonant Charge Transport in Conjugated Molecular Wires Beyond 10 nm Range. *Journal of the American Chemical Society* **2016**, *138*, 11140-11143.
- 30. Michaeli, K.; Beratan, D. N.; Waldeck, D. H.; Naaman, R. Voltage-Induced Long-Range Coherent Electron Transfer through Organic Molecules. *Proceedings of the National Academy of Sciences* **2019**, *116*, 5931.
- 31. Akkaoui, K.; Yang, M.; Digby, Z. A.; Schlenoff, J. B. Ultraviscosity in Entangled Polyelectrolyte Complexes and Coacervates. *Macromolecules* **2020**, *53*, 4234-4246.
- 32. Coughlin, J. E.; Reisch, A.; Markarian, M. Z.; Schlenoff, J. B. Sulfonation of Polystyrene: Toward the "Ideal" Polyelectrolyte. *J Polym Sci Pol Chem* **2013**, *51*, 2416-2424.
- 33. Fares, H. M.; Wang, Q.; Yang, M.; Schlenoff, J. B. Swelling and Inflation in Polyelectrolyte Complexes. *Macromolecules* **2019**, *52*, 610-619.
- 34. Shamoun, R. F.; Hariri, H. H.; Ghostine, R. A.; Schlenoff, J. B. Thermal Transformations in Extruded Saloplastic Polyelectrolyte Complexes. *Macromolecules* **2012**, *45*, 9759-9767.
- 35. Mueller, R.; Köhler, K.; Weinkamer, R.; Sukhorukov, G.; Fery, A. Melting of PDADMAC/PSS Capsules Investigated with AFM Force Spectroscopy. *Macromolecules* **2005**, *38*, 9766-9771.
- 36. Bard, A. J.; Faulkner, L. R. Electrochemical Methods; 2nd ed.; Wiley: New York, 2001.
- 37. Salloum, D. S.; Schlenoff, J. B. Rectified Ion Currents through Ultrathin Polyelectrolyte Complex: Toward Chemical Transistors. *Electrochem Solid St* **2004**, *7*, E45-E47.
- 38. Feldberg, S. W.; Sutin, N. Distance Dependence of Heterogeneous Electron Transfer through the Nonadiabatic and Adiabatic Regimes. *Chemical Physics* **2006**, *324*, 216-225.
- 39. Velický, M.; Hu, S.; Woods, C. R.; Tóth, P. S.; Zólyomi, V.; Geim, A. K.; Abruña, H. D.; Novoselov, K. S.; Dryfe, R. A. W. Electron Tunneling through Boron Nitride Confirms Marcus—Hush Theory Predictions for Ultramicroelectrodes. *ACS Nano* **2020**, *14*, 993-1002.
- 40. Sato, S.; Iwase, S.; Namba, K.; Ono, T.; Hara, K.; Fukuoka, A.; Uosaki, K.; Ikeda, K. Electrical Matching at Metal/Molecule Contacts for Efficient Heterogeneous Charge Transfer. *ACS Nano* **2018**, *12*, 1228-1235.
- 41. Ghostine, R. A.; Markarian, M. Z.; Schlenoff, J. B. Asymmetric Growth in Polyelectrolyte Multilayers. *Journal of the American Chemical Society* **2013**, *135*, 7636-7646.

- 42. Picart, C.; Mutterer, J.; Richert, L.; Luo, Y.; Prestwich, G. D.; Schaaf, P.; Voegel, J. C.; Lavalle, P. Molecular Basis for the Explanation of the Exponential Growth of Polyelectrolyte Multilayers. *P Natl Acad Sci USA* **2002**, *99*, 12531-12535.
- 43. Picart, C.; Lavalle, P.; Hubert, P.; Cuisinier, F. J. G.; Decher, G.; Schaaf, P.; Voegel, J. C. Buildup Mechanism for Poly(L-Lysine)/Hyaluronic Acid Films onto a Solid Surface. *Langmuir* **2001**, *17*, 7414-7424.
- 44. Zhang, L.; Zheng, M.; Liu, X.; Sun, J. Layer-by-Layer Assembly of Salt-Containing Polyelectrolyte Complexes for the Fabrication of Dewetting-Induced Porous Coatings. *Langmuir* **2010**, *27*, 1346-1352.
- 45. McAloney, R. A.; Sinyor, M.; Dudnik, V.; Goh, M. C. Atomic Force Microscopy Studies of Salt Effects on Polyelectrolyte Multilayer Film Morphology. *Langmuir* **2001**, *17*, 6655-6663.
- 46. Yashiro, J.; Norisuye, T. Excluded-Volume Effects on the Chain Dimensions and Transport Coefficients of Sodium Poly(Styrene Sulfonate) in Aqueous Sodium Chloride. *Journal of Polymer Science Part B: Polymer Physics* **2002**, *40*, 2728-2735.
- 47. Markarian, M. Z.; Hariri, H. H.; Reisch, A.; Urban, V. S.; Schlenoff, J. B. A Small-Angle Neutron Scattering Study of the Equilibrium Conformation of Polyelectrolytes in Stoichiometric Saloplastic Polyelectrolyte Complexes. *Macromolecules* **2012**, *45*, 1016-1024.
- 48. Shamoun, R. F.; Reisch, A.; Schlenoff, J. B. Extruded Saloplastic Polyelectrolyte Complexes. *Advanced Functional Materials* **2012**, *22*, 1923-1931.
- 49. Farhat, T. R.; Schlenoff, J. B. Ion Transport and Equilibria in Polyelectrolyte Multilayers. *Langmuir* **2001,** *17*, 1184-1192.
- 50. Gough, D. A.; Leypoldt, J. K. Membrane-Covered, Rotated Disk Electrode. *Analytical Chemistry* **1979,** *51*, 439-444.
- 51. Ikeda, T.; Schmehl, R.; Denisevich, P.; Willman, K.; Murray, R. W. Permeation of Electroactive Solutes through Ultrathin Polymeric Films on Electrode Surfaces. *Journal of the American Chemical Society* **1982**, *104*, 2683-2691.
- 52. Davies, T. J.; Compton, R. G. The Cyclic and Linear Sweep Voltammetry of Regular and Random Arrays of Microdisc Electrodes: Theory. *Journal of Electroanalytical Chemistry* **2005**, *585*, 63-82.
- 53. Peinetti, A. S.; Gilardoni, R. S.; Mizrahi, M.; Requejo, F. G.; González, G. A.; Battaglini, F. Numerical Simulation of the Diffusion Processes in Nanoelectrode Arrays Using an Axial Neighbor Symmetry Approximation. *Analytical Chemistry* **2016**, *88*, 5752-5759.
- 54. Winkler, J. R.; Gray, H. B. Long-Range Electron Tunneling. *Journal of the American Chemical Society* **2014**, *136*, 2930-2939.
- 55. Becka, A. M.; Miller, C. J. Electrochemistry At Omega-Hydroxy Thiol Coated Electrodes. 3. Voltage Independence of the Electron Tunneling Barrier and Measurements of Redox Kinetics at Large Overpotentials. *The Journal of Physical Chemistry* **1992**, *96*, 2657-2668.
- 56. Morteza Najarian, A.; McCreery, R. L. Structure Controlled Long-Range Sequential Tunneling in Carbon-Based Molecular Junctions. *ACS Nano* **2017**, *11*, 3542-3552.
- 57. Wenger, O. S.; Leigh, B. S.; Villahermosa, R. M.; Gray, H. B.; Winkler, J. R. Electron Tunneling through Organic Molecules in Frozen Glasses. *Science* **2005**, *307*, 99-102.
- 58. Smalley, J. F.; Geng, L.; Chen, A.; Feldberg, S. W.; Lewis, N. S.; Cali, G. An Indirect Laser-Induced Temperature Jump Study of the Influence of Redox Couple Adsorption on Heterogeneous Electron Transfer Kinetics. *Journal of Electroanalytical Chemistry* **2003**, *549*, 13-24.
- 59. Yan, H.; Bergren, A. J.; McCreery, R.; Della Rocca, M. L.; Martin, P.; Lafarge, P.; Lacroix, J. C. Activationless Charge Transport across 4.5 to 22 nm in Molecular Electronic Junctions. *Proceedings of the National Academy of Sciences* **2013**, *110*, 5326-5330.
- 60. Jortner, J.; Bixon, M.; Langenbacher, T.; Michel-Beyerle, M. E. Charge Transfer and Transport in DNA. *Proceedings of the National Academy of Sciences* **1998**, *95*, 12759-12765.
- 61. Wohlgamuth, C. H.; McWilliams, M. A.; Slinker, J. D. DNA as a Molecular Wire: Distance and Sequence Dependence. *Analytical Chemistry* **2013**, *85*, 8634-8640.

- 62. Hong, Y. A.; Hahn, J. R.; Kang, H. Electron Transfer through Interfacial Water Layer Studied by Scanning Tunneling Microscopy. *The Journal of Chemical Physics* **1998**, *108*, 4367-4370.
- 63. Gosavi, S.; Marcus, R. A. Nonadiabatic Electron Transfer at Metal Surfaces. *The Journal of Physical Chemistry B* **2000**, *104*, 2067-2072.
- 64. Renaud, N.; Berlin, Y. A.; Lewis, F. D.; Ratner, M. A. Between Superexchange and Hopping: An Intermediate Charge-Transfer Mechanism in Poly(a)-Poly(T) DNA Hairpins. *Journal of the American Chemical Society* **2013**, *135*, 3953-3963.
- 65. Schuster, G. B. Long-Range Charge Transfer in DNA: Transient Structural Distortions Control the Distance Dependence. *Accounts of Chemical Research* **2000**, *33*, 253-260.
- 66. Conwell, E. M.; Rakhmanova, S. V. Polarons in DNA. *Proceedings of the National Academy of Sciences* **2000**, *97*, 4556-4560.
- 67. Crank, J. *The Mathematics of Diffusion*; Clarendon Press: Oxford, 1975.
- 68. Ball, V.; Duval, J. F. L. Ultra-Slow Diffusion of Hexacyanoferrate Anions in Poly(Diallyldimethyl Ammonium Chloride)-Poly(Acrylic Acid Sodium Salt) Multilayer Films. *Journal of Colloid and Interface Science* **2019**, *539*, 306-314.
- 69. Lu, Q.; Liu, K.; Zhang, H.; Du, Z.; Wang, X.; Wang, F. From Tunneling to Hopping: A Comprehensive Investigation of Charge Transport Mechanism in Molecular Junctions Based on Oligo(P-Phenylene Ethynylenes). *ACS Nano* **2009**, *3*, 3861-3868.
- 70. Beratan, D. N. Why Are DNA and Protein Electron Transfer So Different? *Annual Review of Physical Chemistry* **2019**, *70*, 71-97.
- 71. Chien, J. C. W. *Polyacetylene. Chemistry, Physics, and Materials Science*; Academic Press: Orlando, 1984.